

Shock Initiation of Explosives through Shock Wave-Induced Electrical Breakdown

Yuanjie Huang^{1, 2*}, Zhiqiang Chen^{2*}

¹ *Chinese Academy of Engineering Physics, Mianyang 621900, China*

² *Center for High Pressure Science and Technology Advanced Research, Shanghai 201203, China*

*Corresponding Authors' E-mails: hyj201207@163.com; chenzq@hpstar.ac.cn

Shock initiation of high explosive (HE) is very important for both the civilian and defense communities, and the hotspot mechanism has been widely recognized as the dominant regime. However, how the hotspots can generate conspicuous reaction of the surrounding bulk HE has still been a challenging topic in recent decades. In this work, using the physics of shock polarization and *Yuheng Zhang equation*, the shock wave-induced electrical breakdown (SWIEB) mechanism and the related chemical reaction rate equation was proposed for shock initiation of HE. It was found that the SWIEB mechanism agreed with most experimental observations on the shock initiation phenomena. As indicated by the performed experiments on the electrical breakdown of ammonia borne (NH_3BH_3) in this work, the electrical breakdown cannot only remarkably accelerate the reaction rate even at room temperature but also result in a reaction route different from the thermal reaction route, thereby yielding distinct reaction products. The experimental results suggested that the SWIEB may be an important and rational mechanism for the reaction of bulk HE around the hotspots. Overall, the proposed SWIEB may pave a new and reasonable way of understanding

the physics of shock initiation and may help people design much safer HE in both the civilian and defense fields.

keywords: high explosive; shock initiation; shock wave; electrical breakdown; hotspots; chemical reaction rate;

1. Introduction

The high explosive (HE) is important for not only the civilian but also the defense communities. The shock initiation of HE usually sensitively depends on the characteristics of HE under shock loading, especially the initial defects which can generate many hotspots. The hotspots are regions of HE with high temperature and reactivity, and they have been widely recognized as the most important regime of shock initiation [1, 2, 3]. The hotspot formation mechanism is of paramount importance and is a hot topic. Many different mechanisms have been proposed for the hotspot formation when the HE is subject to shock waves, *e.g.*, pore collapse [3, 4], pressure fluctuation [5, 6], nanoscale shear band [7], electric discharges [8] and a large number of other candidates [9, 10]. The pore collapse mechanism has attracted the most attention and is commonly regarded as the dominant hotspot mechanism [11-15] because the shock initiation sensitively depend on the porosity of HE [3, 16, 17]. Regardless of the formation mechanism, only the active hotspots satisfying the critical hotspot criterion which requires the sufficiently large size, high enough temperature and adequate duration [3] can be of paramount importance. The active hotspots can induce the chemical reactions of the HE in the hotspots, and the yielded heat could be thermally conducted to the neighboring cooler bulk HE. Hence, the chemical reaction rate of the bulk HE around the hotspot may be improved due to the temperature increase. Only when the proportion of the reacted HE reaches a very notable fraction, can the shock wave grow into a detonation wave.

The problem is how the hotspots can give rise to the detonation. The physics of

hotspots and the induced reaction mechanism of bulk HE around the hotspot is still a challenging forefront scientific topic [3]. Upon the problem, based on the famous Arrhenius equation, it was popularly assumed that the chemical reaction rate of HE outside the hotspot could be improved by the temperature rise induced by the thermal conduction from the hotspots. The related modeling approaches such as the mesoscale modeling [3, 18, 19, 20] has attracted much attention. But the thermally induced chemical reaction of the bulk HE may not be dramatic enough to cause the detonation initiation. Because the thermal conductivity of HE is usually so small that the temperature rise of the bulk HE in the neighborhood of hotspots during the run to detonation time cannot cause the severe chemical reactions and the induced burn front speed may be too low to cause shock initiation [20]. A simple estimation could be performed here. The order of thermal conductivity of HE is $\lambda \sim 1 \text{ W/m/K}$ [21], the density order $\rho \sim 10^3 \text{ kg/m}^3$ [4], and the order of heat capacity of HE is $C_V \sim 10^3 \text{ J/kg/K}$ [4, 22]. The spatial scale of the thermally affected regions in the vicinity of a hotspot may be only $\sqrt{\lambda t_r / \rho C_V} \sim 10^{-6} \text{ m}$ where the t_r is the run to detonation time which is usually less than 10 us [3, 23]. The thermally affected regions around a hotspot may be too small to cause the shock initiation. Therefore, for the shock initiation, besides the thermal conduction, there may exist other important hotspot mechanisms accelerating the chemical reaction rate of the surrounding bulk HE.

In this work, a new mechanism leading to the substantial reaction of bulk HE around the hotspots, which was distinct from the conventional thermal conduction mechanism, was proposed. It was found that the new mechanism agreed with most previously

known experimental results.

2. Experimental results and discussion

When the shock wave propagated into the liquids and solids, an electromotive force (EMF) and an electrical current were found to appear across the shock wave front and the related phenomena was named after shock polarization in literatures [24]. The shock polarization was non-equilibrium phenomena and could be interpreted by means of the *Yuheng Zhang equation* [25]

$$\nabla E_F(\vec{r}) = e\vec{E} \quad (1)$$

where E_F is position-dependent electron (positron) chemical potential and it is also known as Fermi level instead of Fermi energy, e electron charge, \vec{E} the electric field. Upon strains, the strain-induced electric field could be obtained by means of Equation (1) and it is

$$\vec{E} = \frac{1}{e} \frac{\partial E_F(\vec{r})}{\partial \xi_{ij}} \nabla \xi_{ij} \quad (2)$$

where \vec{E} is the electric field, ξ_{ij} are the strains where the indices are $i, j=x, y, z$ and obey Einstein summation convention, $\partial E_F(\vec{r})/\partial \xi_{ij}$ the mechanical-electric coupling strength. Upon shock wave loading, the EMF was given by [25]

$$eV_m = E_F(\xi_2) - E_F(\xi_1) \quad (3)$$

where V_m is the EMF across the shock wave front, $E_F(\xi_2)$ the Fermi level of the compressed material behind the shock wave, $E_F(\xi_1)$ the Fermi level of the uncompressed material before the shock wave. For the HE under the shock waves, the strain behind the shock waves usually reach $\sim 10\%$ in the explosive. Based on the experimental results of shock polarization, the EMF may approach 0.1-1 V and the

strength of the effective electric field (EEF) in the shock wave front may reach the order of 10^8 V/m. The EMF and intensive EEF may activate the space charges and the weakly trapped electrons in the HE, thereby causing the electrical breakdown in the explosive. The remarkable electrical breakdown will consequently give birth to fierce chemical reaction in the HE, resulting in the detonation at last, and the experimental proof for the electrical breakdown enhancing chemical reaction rate will be deferred in the next section. This is the main point of the proposed shock wave-induced electrical breakdown (SWIEB) in this work. Very interestingly, SWIEB was found to agree well with most phenomena on sensitivity of HE, and the related factors such as the temperature, the impurity particles, the cavities, the porosity and the strain gradient would be discussed in the followings.

For the HE under the shock wave, the temperature usually increases. The increase of the temperature may have two positive effects on promoting the chemical reaction rate. One is that the chemical reaction rate is usually improved greatly with the increase of the temperature according to the Arrhenius's law. The other is that the electrical breakdown strength (EBS) of HE is usually reduced dramatically as the temperature increases. Since a stronger shock wave usually causes a larger increase of temperature, the chemical reaction rate could be accelerated more substantially for the HE under stronger shock wave.

Any method which can either improve the EEF or reduce the EBS may facilitate the electrical breakdown of HE. For instance, when the HE would be loaded by a shock wave, the existence of high shock-impedance particles or sheets in the HE could yield

a stronger shock wave reflecting from these interfaces between the HE and the high shock-impedance particles or sheets. The stronger shock wave may give birth to a larger EMF and EEF across the shock wave front, which may be easy to cause the electrical breakdown of HE. So the materials with high shock-impedance such as quartz sands and broken glass could usually be utilized as sensitizer for HE, which is in accord with experimental results [26]. On the contrary, for the HE added by the materials with low shock-impedance, when the HE would be loaded by a shock wave, the rarefaction waves will be created at the interfaces between the HE and the low shock-impedance material. The rarefaction waves may result in decrease of both the temperature and the EEF in the wave fronts, so it will be difficult for the electrical breakdown to happen in the HE. Hence, the materials such as paraffin and high polymer possessing low shock-impedance could be used as desensitizer for the HE, which agrees with the commonly experimental results [26].

Upon shock wave loading, the HE with a cavity or a bubble can generate a hotspot and a pore-collapse shock wave reflecting into the hotspot [3, 4]. Therefore, according to Equation (2), the yielded EEF within the reflected shock wave front may be enhanced but EBS of HE in the hotspots may be weakened obviously by the high temperature. As a result, the existence of cavities and bubbles in the HE could be easy to induce the electrical breakdown when the HE is loaded by a shock wave.

For the HE with high porosity, upon the loading of a shock wave, many hotspots may be created at the sites of the initial pores. The hotspots usually present both a high temperature and a notable EEF due to the reflected shock wave. So it may be much

easier to cause the electrical breakdown of the HE in the regions of hotspots than other regions. Reversely, for the HE with low porosity, when it would be loaded by a shock wave, the yielded number of hotspots showing not only high temperature but also large EEF may be much less than that with high porosity. In addition, it was established that the pores in a solid can offer little resistance to electrical breakdown and the EBS rapidly declines with increasing porosity [26]. Therefore, the electrical breakdown-induced chemical reaction in the high-porosity HE may be much more noticeable than that in the low-porosity HE. As a result, the HE with high porosity usually exhibits high sensitivity, which is in accord with most experimental results [26].

Based on Equation (2), the EEF in the HE under the mechanical loading sensitively depends on the strain gradient. A larger strain gradient can usually induce a stronger EEF. So the EEF in the shock wave front may be much larger than that in the quasi-isentropic compression wave front even if the eventually accomplished compressive strain is the same for both the shock wave and the quasi-isentropic compression wave. Thus, the possibility for the electrical breakdown to occur in the HE under shock wave loading may be much larger than that under the quasi-isentropic compression wave loading. As a result, the detonation initiation is easier to happen for the HE under the shock wave than that under quasi-isentropic compression wave, which is the commonly encountered experimental observations.

The shock desensitization is very common and usually covers two topics [3]. One is that the reaction behind the second shock wave following the first shock wave in HE is lacking. The other is that a detonation wave in HE could extinct when the detonation

wave interact with a shock wave. The widely accepted explanation is that it is difficult for the second shock wave to activate the hotspots activated by the first shock wave, thereby desensitizing the HE [2]. Another explanation is that the entropy and the temperature caused by multiple shock waves may be much lower than that induced by a single shock wave to the same pressure [28]. Here another mechanism of shock desensitization was proposed in terms of the SWIEB. For the HE compressed by the first shock wave, when the second shock wave arrives, the created EEF at the second shock wave front may be much smaller than that at a single shock wave front to the same pressure. In addition, the HE experiencing a weak shock wave may exhibit a larger EBS because of the porosity dropping. Therefore, the possibility for the yielded EEF exceeding the EBS of the HE compressed by the first weak shock wave may remarkably decrease, which renders the HE less reactive and leads to the shock desensitization.

Despite the unsolved electrical breakdown mechanism in different types of insulating liquids and solids [29], it was established that the related electrical breakdown channels are usually electrically conductive [30, 31]. For the shock initiation of HE, if the SWIEB mechanism is indeed important, to be expected and inferred, the chemical reaction products would be electrically conductive. It is in agreement with the well-designed experiments showing that the reaction zones behind detonation fronts is electrically conductive [32, 33].

The electrical breakdown-induced reaction products is distinct from the thermally reacted products, as will be shown in the following experiments. Therefore,

if the shock initiation of HE is only thermally activated by hotspots, the reaction products will be almost the same as that released by HE under high temperatures solely. Reversely, if the electrical breakdown mechanism can dominate the chemical reaction of HE, the kinds and amounts of the reacted products behind the detonation zone will be very different.

Through the former discussions on the sensitivity of HE, interestingly, the SWIEB mechanism was revealed to be in accord with the experimental results on the influencing factors of the shock initiation, *e.g.*, the temperature, the impurity particles, the cavities, the porosity, the strain gradient and the shock desensitization. Therefore, the SWIEB-induced reaction rate of HE may be important for the shock initiation, and it should be explored further in the following parts.

The electrical breakdown channels was found to exhibit the fractal structure and the fractal properties of electrical breakdown channels was investigated in a plane [34]. Analogously, the electrical breakdown channels in HE may present the fractal patterns and the total area of the breakdown channels could be written as

$$S(t) = A_0 [r(t)]^d \quad (4)$$

where $S(t)$ is the time-dependent total area of the breakdown channels, $r(t)$ denotes the time dependence of the total length of the breakdown channels, A_0 a time-independent parameter, d stands for the fractal dimension and it usually fulfill the relation $2 \leq d \leq 3$.

The chemical reaction rate may strongly rest with the expanding speed of the breakdown channels, and the related reaction volume versus time for a single breakdown channel may be obtained

$$\frac{\partial V(t)}{\partial t} = k_0 d [r(t)]^{d-1} \frac{\partial r(t)}{\partial t} p(E - E_B(T, P, t)) \quad (5)$$

where $V(t)$ denotes the time-dependent volume of chemically reacted HE induced by electrical breakdown, k_0 the pre-exponential factor depending upon the intrinsic features of HE, and it usually contains the information of the breakdown channel thickness and the order of the reaction, $p(E - E_B(T, P, t))$ is the probability function of electrical breakdown, where E is the EEF and $E_B(T, P, t)$ is the temperature, pressure and time dependence of EBS. The probability function is 1 if the EEF exceeds the breakdown strength $E_B(T, P, t)$, otherwise it is zero, *i.e.*, $p=1$ if $E \geq E_B(T, P, t)$ and $p=0$ if $E < E_B(T, P, t)$.

When the real electrical breakdown occurs in the vicinity of hotspots, many electrical breakdown channels may be generated. The corresponding totally reacted volume could be expressed as

$$\frac{\partial V(t)}{\partial t} = \sum_{i=1}^{i=N} k_0 d_i [r_i(t)]^{d_i-1} \frac{\partial r_i(t)}{\partial t} p_i(E - E_B(T, P, t)) \quad (6)$$

where $V(t)$ signifies the totally reacted volume of HE, k_0 the pre-exponential factor, d_i is the fractal dimension of the *i*th breakdown channel, $r_i(t)$ denotes the time dependence of the length of the *i*th breakdown channel, $p_i(E - E_B(T, P, t))$ is the probability function of the *i*th electrical breakdown channel.

To show the electrical breakdown mechanism accelerating the reaction rate of reactants, the experiment that the ammonia borane (AB= NH_3BH_3) subject to electrical breakdown was performed. AB is one of the chemical hydrogen storage materials, and has attracted increasing attention due to its high hydrogen capacity which is crucial for

potential transportation applications (19.6 wt %). It has promising commercial availability, well-behaved stability under room conditions, and intriguing chemical and physical properties, but its slow hydrogen releasing rate is the foremost challenge for practical applications. Until now several primary but problematic strategies such as solid state thermolysis, metal-catalyzed dehydrogenation [35-51], nanoscaffold [52-56] and solution thermolysis [57-59] have been utilized. For solid state thermolysis, only when AB is heated above 150 °C does its decomposition yield more than one equivalent of hydrogen molecules [60]. This thermal dehydrogenation method does not need a catalyst, however, its main drawbacks are the slow release rate of H₂ and the high reaction temperatures which exceed the operating temperature of fuel cells, and impede its practical usages. Here, it would be experimentally demonstrated that the electrical breakdown enables its hydrogen releasing kinetics to dramatically improve even at room temperature.

In the experiments, AB powders (CAS No. 13774-81-7) were purchased from Zhengzhou Alfa Aesar with stated purity 98%. The pristine AB powders were characterized by Raman and infrared spectrum to check the quality. In order to examine the hydrogen releasing rate of AB under electrical breakdown, the AB powders were compressed into some thin slices (about 200-300 microns thick) by a steel mould. Due to the softness of AB, the density of these slices almost approached that of AB crystal. Then the slice was placed between two thin metal plates which were utilized as electrodes. An external electrical voltage could be applied between the electrodes, thereby applying an electric field for the AB slices. The sample and electrodes were put

in a sealed metal apparatus. The releasing gas was collected by using the conventional volumetric-release method. The time dependence of the relative yield releasing from AB was diagnosed by the gas chromatography-mass spectrometry.

To examine the quality of the pristine AB, the Raman and Infrared experiments were carried out and the results were shown in Figure S1 and Figure S2. These spectrums are in good agreement with previous reports [61, 62], approving the quality and purity of the samples.

The dehydrogenation of AB under electrical breakdown were investigated at various temperatures utilizing the volumetric-release techniques, wherein the electrical breakdown fields at different temperatures range from 1×10^6 V/m to 5×10^6 V/m. As shown in Figure 1, excitingly, upon electrical breakdown and without any catalyst the obtained hydrogen releasing rate from AB is promoted greatly and the evolution extent reaches near two equivalents of hydrogen even at room temperature. The hydrogen releasing process may experience two stages. In the first stage, the hydrogen releasing rate decreases with the increasing temperature, but it seems to remain the same in the second stage. This hydrogen releasing rate is the fastest among all the solid state decomposition methods such as thermolysis [63] and nano-scaffold [52, 55]. It is entirely comparable with the results achieved by the action of metal catalysts in solution, but unlike metal catalysts, nanoscaffold and solutions, here the efficient hydrogen weight is barely sacrificed.

During the hydrogen releasing processes, unlike thermolysis with notable foaming and volume expansion (see Figure S3(b)), non-foamed solid products are observed

under electrical breakdown (see insets of Figure S3(a)), indicating a distinct reaction route from thermolysis. When the temperature changes, very interestingly and surprisingly, the obtained hydrogen releasing rate increases as the temperature decreases (as shown in Figure 1), suggesting this abnormal hydrogen releasing mechanism to be induced by the electrical breakdown not by the thermolysis. When the electrical breakdown occurs, the space charges and lowly trapped electrons may be accelerated to a high velocity by the strong electric field within the breakdown channels. These high-speed electrons may collide with the AB molecules and consequently activate them by means of energy transfer between the electrons and AB molecules, as may assist these AB molecules in overcoming decomposition energy barrier and result in the fast release of hydrogen. Here the electrical breakdown is different from the electrolysis, because: 1) electrolysis happens in molten or ionic solutions, but electrical breakdown occurs for AB in the solid state; and 2) the chemical reaction induced by the electrolysis usually takes place at the surfaces of the electrodes, while the hydrogen releasing processes caused by the AB electrical breakdown mainly exist at the breakdown channels in the interior of AB samples (the brown products are shown in Figure S3(a)).

In the series of experiments, the aluminum plates were used as the raw electrodes and though they possess large masses, they can be optimized so that the effective hydrogen storage of AB does not drop, e.g. two conductive thin films were utilized as the electrodes. The hydrogen releasing rate versus the efficient hydrogen storage weight percentage (wt %) achieved in both the previous work [43-46, 50-52, 54-56, 59, 60, 64,

65] and this work are summarized in Figure 2. From this figure, the electrical breakdown method exhibits the optimum behaviors: both in fast hydrogen releasing rate and highly efficient hydrogen storage weight.

The *in situ* Mass Spectroscopy experiments under thermolysis and electrical breakdown were performed to detect the volatile products, as shown in Figure 3. As the temperature decreases, against the notable emission of the volatile gases such as ammonia under thermolysis [55] (see Figure 3c), the relative yield of ammonia under electrical breakdown is prominently reduced (see Figure 3a and 3b). This implies that the chemical decomposition is sensitive to temperature, and the formation of H₂ from the AB molecules is superior to the formation of ammonia arising from the N-B bond breaking under electrical breakdown, especially at low temperatures.

To examine the products further, we carried out the Raman experiments for the series of products under thermolysis and electrical breakdown. Our data are summarized in Figure S4. It can be seen that the Raman spectrum of the products under electrical breakdown is quite different from that under thermolysis. For all the electrical breakdown products, the symmetric and asymmetric stretching modes for N-H at 3200 cm^{-1} and B-H at 2400 cm^{-1} [61] are greatly weakened, and the -NH₃ and -BH₃ deformation modes between 1000 and 1600 cm^{-1} are also suppressed. The weakening of these vibration modes suggests that electrical breakdown causes higher hydrogen desorption extent than thermolysis, which is consistent with the experimental results shown in Figure 1.

Nevertheless, the unique features of the electrical breakdown method should be

reexamined. First, this method could cause the highly efficient hydrogen release from AB and might be applicable to other chemical hydrogen storage materials. Second, a combination of this method and other methods, e.g. nanoscaffold may promote the hydrogen release further. Third, some electrical energy is consumed in the electrical breakdown processes (see Figure S5), which must be overcome in the future. Fourth, the electrical breakdown method may be a natural and vital way for facilitating some types of chemical reactions in some areas.

The experimental results on AB under electrical breakdown proved that the electrical breakdown mechanism can accelerate the chemical reaction rate greatly even at the relatively low temperatures. It also indicated that the reaction route of the reactant under electrical breakdown was distinct from that of the reactant under thermolysis. It further revealed that the reaction products under electrical breakdown differed from that under thermolysis.

At last, some comments on the SWIEB mechanism were made. The proposed SWIEB mechanism for the shock initiation of HE may exhibit some interesting and unique characteristics. Firstly, what leads to the electrical breakdown of HE is the intrinsically intensive EEF which is induced by the shock wave rather than the externally applied electric field. It may be the reason that the electrical breakdown was known to cause chemical reaction long ago but was not utilized to investigate the shock initiation of HE. Secondly, the electrical breakdown enables the HE to accelerate the reaction rate very obviously at temperatures much lower than that needed for the thermal reaction of HE. The number, fractal dimension and expanding speed of the

breakdown channels may be the main factors monitoring the reaction rate of HE. Thirdly, in the case of HE under shock wave loading, whether the electrical breakdown happens or not sensitively depends on the microstructure of HE and the properties of the loaded shock wave but is not much relevant to the molecular structure of the HE molecules. Fourthly, the electrical breakdown usually displays the statistical characteristics, so the probability had better be used to describe the event of HE under specific loading conditions. Fifthly, the SWIEB might be a relatively universal method and could be employed to catalyze other types of important chemical reactions at milder conditions. Sixthly, despite the proposed SWIEB in this work, the detailed physical and chemical processes responsible for the reaction of bulk HE around hotspots still need to be investigated very carefully in the future. Seventhly, the SWIEB could be utilized to explore next-generation safe and insensitive HE. According to Equation (2) and SWIEB, it could be inferred that the HE exhibiting a smaller mechanical-electric coupling strength could be more insensitive to shock waves if no phase transition happens during the process. It could also be implied that the HE presenting less space charges, less lowly-trapped electrons, weaker low-frequency (<100 MHz) dielectric responses, smaller temperature dependence of EBS and higher EBS could be much more insensitive and much safer in various applications.

3. Conclusions

In summary, the SWIEB mechanism was proposed for shock initiation of HE based on the shock polarization and *Yuheng Zhang equation* in this work. Through analysis, the SWIEB mechanism was found to be consistent with most known experimental results

of the shock initiation phenomena. Demonstrated by the experimental observations on the electrical breakdown of ammonia borne (NH_3BH_3) in the work, the electrical breakdown can remarkably improve the reaction rate and lead to a different reaction route. The experimental observations in this work and the consistency between the SWIEB and the known experimental results proved that the SWIEB may be the mechanism responsible for the fast reaction of bulk HE around the hotspots. In a word, the proposed SWIEB may help people understand the shock initiation mechanism and guide people to design and manufacture much safer HE in related areas.

References:

- [1] A. W. Campbell, W. C. Davis, and J. R. Travis, "Shock initiation of liquid explosives," *Phys. Fluids* 4, 498–510 (1961).
- [2] A. W. Campbell, W. C. Davis, J. B. Ramsay, and J. R. Travis, "Shock initiation of solid explosives," *Phys. Fluids* 4, 511–521 (1961).
- [3] C. A. Handley, B. D. Lambourn, N. J. Whitworth, H. R. James, W. J. Belfield, Understanding the shock and detonation response of high explosives at the continuum and meso scales, *Appl. Phys. Rev.* V. 5, 011303(1-65) (2018).
<https://doi.org/10.1063/1.5005997>.
- [4] 章冠人, 陈大年, 凝聚炸药起爆动力学, 北京: 国防工业出版社, 第一版, 1991, pp.113-127.
- [5] Khokhlov, A. M. and Oran, E. S. Numerical simulation of detonation initiation in flame brush: the role of hot spots. *Combustion and Flame*, 119(4):400-416(1999).
- [6] Oran, E. S. and Khokhlov, A. M. Deflagrations, hot spots, and the transition to detonation. *Philosophical Transactions of the Royal Society of London A: Mathematical, Physical and Engineering Sciences*, 357(1764):3539-3551(1999).
- [7] Matthew P. Kroonblawd Laurence E. Fried, High Explosive Ignition through Chemically Activated Nanoscale Shear Bands, V. 124, 206002(1-6) (2020).
- [8] R. M. H. Wyatt, P. W. J. Moore, G. K. Adams, J. F. Sumner, The Ignition of Primary Explosives by Electric Discharges, *Proc. R. Soc. Lond. A* **246**, 189-196(1958).
- [9] J. E. Field, N. K. Bourne, S. J. P. Palmer, and S. M. Walley, Hot spot ignition mechanisms for explosives and propellants, *Philos. Trans. R. Soc. London A* 339, 269–

283 (1992).

[10] J. E. Field, Hot spot ignition mechanisms for explosives, *Acc. Chem. Res.* 25, 489–496 (1992).

[11] M. A. Wood, M. J. Cherukara, E. M. Kober, A. Strachan, Ultrafast Chemistry under Nonequilibrium Conditions and the Shock to Deflagration Transition at the Nanoscale, *J. Phys. Chem. C* 119, 22008-22015 (2015).

[12] R. M. Eason and T. D. Sewell, Molecular Dynamics Simulations of the Collapse of a Cylindrical Pore in the Energetic Material α -RDX *J. Dyn. Behav. Mater.* 1, 423-438(2015).

[13] H. K. Springer, S. Bastea, A. L. Nichols III, C. M. Tarver, J. E. Reaugh, Modeling The Effects of Shock Pressure and Pore Morphology on Hot Spot Mechanisms in HMX, *Propellants Explos. Pyrotech.* 43, 805-817 (2018).

[14] N. K. Rai and H. S. Udaykumar, Void collapse generated meso-scale energy localization in shocked energetic materials: Non-dimensional parameters, regimes, and criticality of hotspots, *Phys. Fluids* 31, 016103(2019).

[15] P. Zhao, S. Lee, T. Sewell, and H. S. Udaykumar, Tandem Molecular Dynamics and Continuum Studies of Shock-Induced Pore Collapse in TATB Propellants *Explos. Pyrotech.* 45, 196-222 (2020).

[16] N. K. Bourne, A. M. Milne, The temperature of a shock-collapsed cavity, *Proc. R. Soc. London A* V. 459, 1851–1861 (2003).

[17] L. E. Fried, F. Najjar, W. M. Howard, M. R. Manaa, E. J. Reed, N. Goldman, S. Bastea, A. L. Nichols III, Multiscale simulation of hot spot ignition, in Fourteenth

International Detonation Symposium (Office of Naval Research, 2010), pp. 1412–1420.

[18] P. A. Conley, Eulerian hydrocode analysis of reactive micromechanics in the shock initiation of heterogeneous energetic material, Ph.D. thesis (University of California, San Diego, Department of Mechanical Engineering, 1999).

[19] N. J. Whitworth, “Mathematical and numerical modelling of shock initiation in heterogeneous solid explosives,” Ph.D. thesis (Defence College of Science & Technology, Cranfield University, 2008), <http://hdl.handle.net/1826/2772>.

[20] C. A. Handley, Numerical modelling of two HMX-based plastic-bonded explosives at the mesoscale, Ph.D. thesis (University of St Andrews, 2011), <http://hdl.handle.net/10023/1709>.

[21] Xilin Yan, Shimin Zhang, Wei Tang, Minggang Xia, Thermal Conductivity of PBX Calculated by Phonons of Explosive and Binder Molecular Crystals, *ES Energy Environ.*, V. 11, 74-83(2021).

[22] Zhongqing Wu, Weiwei Mou, Rajiv K. Kalia, Aiichiro Nakano, Priya Vashishta, Vibrational and Thermodynamic Properties of 1,3,5-Triamino-2,4,6-Trinitrobenzene (TATB): Comparison of Exchange-Correlation Functionals in Density Functional Theory, *International Journal of Energetic Materials and Chemical Propulsion*, 14 (6): 519–547 (2015).

[23] T. R. Gibbs, A. Popolato, *LASL Explosive Property Data*, University of California Press, 1980.

[24] V. N. Mineev and A. G. Ivanov, Electromotive force produced by shock compression of a substance, *Sov. Phys. Usp.*, **19**, No. 5, 400-419 (1976).

- [25] Yuanjie Huang, Strain Induced Electric Effect in Condensed Matters, *Journal of Materials Sciences and Applications*, **5**(3), 44-57(2019).
- [26] Yuanjie Shu, Jichuan Huo, *Introduction to explosives*, Beijing: Chemical industry press, 2011, pp.87-91.
- [27] Robert Gerson, Thomas C. Marshall, Dielectric breakdown of porous ceramics, *J. Appl. Phys.* V. 30, 1650-1653(1959).
- [28] H. R. James, B. D. Lambourn, Shock desensitization in explosives: An exploration of two competing hypotheses, in *Fourteenth International Detonation Symposium* (Office of Naval Research, 2010), Vol. ONR 351-10-185, pp. 1172–1181.
- [29] E. Kuffel, W. S. Zaengl, J. Kuffel, *High Voltage Engineering*, Butterworth-Heinemann, 2000, pp.367-393.
- [30] S. Chiang, R. Wang, T. Speers, J. McCollum, E. Hamdy, C. Hu, Conductive Channel in ONO Formed by Controlled Dielectric Breakdown, *Symposium on VLSI Technology Digest of Technical papers*, 20-21, 1992.
- [31] Masayuki Ieda, Dielectric Breakdown Process of Polymers, *IEEE Transactions on Electrical Insulation* V. EI-15, 206-224, 1980.
- [32] A.P. Ershov, N.P. Satonkina, Electrical conductivity distributions in detonating low-density explosives-Grain size effect, *Combustion and Flame* 157, 1022-1026 (2010).
- [33] Alexander P. Ershov, Natalia P. Satonkina, Gennady M. Ivanov, Reaction zones and conductive zones in dense explosives, *thirteenth international detonation symposium*, 79-88, 2006.

- [34] L. Niemeyer, L. Pietronero, H. J. Wiesmann, Fractal dimension of dielectric breakdown, *Phys. Rev. Lett.* V. **52**, 1033-1036(1984).
- [35] Melanie C. Denney, Vincent Pons, Travis J. Hebden, D. Michael Heinekey, and Karen I. Goldberg, Efficient catalysis of ammonia borane dehydrogenation, *J. Am. Chem. Soc.* 128(2006)12048-12049.
- [36] C.F. Yao, L. Zhuang, Y.L. Cao, X.P. Ai, H.X. Yang, Hydrogen release from hydrolysis of borazane on Pt- and Ni-based alloy catalysts, *International Journal of Hydrogen Energy* 33(2008)2462-2467.
- [37] Arshad Aijaz *et al.* Immobilizing highly catalytically active Pt nanoparticles inside the pores of metal.organic framework: a double solvents approach. *J. Am. Chem. Soc.* 134(2012)13926-13929.
- [38] Feyyaz Durap, Mehmet Zahmakiran, Saim Özkar, Water soluble laurate-stabilized rhodium (0) nanoclusters catalyst with unprecedented catalytic lifetime in the hydrolytic dehydrogenation of ammonia-borane *Applied Catalysis A: General* 369(2009)53-59.
- [39] Feyyaz Durap, Mehmet Zahmakiran, Saim Özkar, Water soluble laurate-stabilized ruthenium(0) nanoclusters catalyst for hydrogen generation from the hydrolysis of ammonia-borane: High activity and long lifetime, *International Journal of Hydrogen Energy* 34(2009)7223-7230.
- [40] Giovanni P. Rachiero, Umit B. Demirci, Philippe Miele, Facile synthesis by polyol method of a ruthenium catalyst supported on γ -Al₂O₃ for hydrolytic dehydrogenation of ammonia borane, *Catalysis Today* 170(2011)85-92.

- [41] Serdar Akbayrak and Saim Özkaz, Ruthenium(0) nanoparticles supported on multiwalled carbon nanotube as highly active catalyst for hydrogen generation from ammonia-borane. *ACS Appl. Mater. Interfaces* 4(2012) 6302-6310.
- [42] Hongyan Liang *et al.* In situ facile synthesis of ruthenium nanocluster catalyst supported on carbon black for hydrogen generation from the hydrolysis of ammonia-borane. *International Journal of Hydrogen Energy*. 37(2012)17921-17927.
- [43] Richard J. Keaton, Johanna M. Blacquiere, and R. Tom Baker, Base metal catalyzed dehydrogenation of ammonia-borane for chemical hydrogen storage, *J. Am. Chem. Soc.* 129(2007)1844-1845.
- [44] Önder Metin, Vismadeb Mazumder, Saim Özkaz, and Shouheng Sun, Monodisperse nickel nanoparticles and their catalysis in hydrolytic dehydrogenation of ammonia borane *J. Am. Chem. Soc.* 132(2010)1468-1469.
- [45] Önder Metin, Saim Özkaz, and Shouheng Sun, Monodisperse nickel nanoparticles supported on SiO₂ as an effective catalyst for the hydrolysis of ammonia-borane *Nano Res.* 3(9)(2010) 676-684.
- [46] Tetsuo Umegaki, Qiang Xu, Yoshiyuki Kojima, Effect of l-arginine on the catalytic activity and stability of nickel nanoparticles for hydrolytic dehydrogenation of ammonia borane. *Journal of Power Sources* 216(2012) 363-367.
- [47] KwangSup Eom, KeunWoo Cho, HyukSang Kwon, Hydrogen generation from hydrolysis of NH₃BH₃ by an electroplated CoCP catalyst. *International Journal of Hydrogen Energy*. 35(2010)181-186.
- [48] Murat Rakap, Saim Özkaz. Hydrogen generation from the hydrolysis of ammonia-

borane using intrazeolite cobalt(0) nanoclusters catalyst. *International Journal of Hydrogen Energy*. 35(2010)3341-3346.

[49] Tetsuo Umegaki *et al.* CoCSiO₂ nanosphere-catalyzed hydrolytic dehydrogenation of ammonia borane for chemical hydrogen storage. *Journal of Power Sources* 195(2010)8209-8214.

[50] Ping Song *et al.* A highly efficient Co (0) catalyst derived from metal-organic framework for the hydrolysis of ammonia borane. *International Journal of Hydrogen Energy*. 36(2011)10468-10473.

[51] Jun-Min Yan, Xin-Bo Zhang, Hiroshi Shioyama, Qiang Xu, Room hydrolytic dehydrogenation of ammonia borane catalyzed by Co nanoparticles, *Journal of Power Sources* 195(2010)1091-1094.

[52] Anna Gutowska *et al.* Nanoscaffold mediates hydrogen release and the reactivity of ammonia borane, *Angew. Chem. Int. Ed.* 44(2005)3578-3582.

[53] Zhongyue Li, Guangshan Zhu, Gaoqing Lu, Shilun Qiu, and Xiangdong Yao, Ammonia borane confined by a metal-organic framework for chemical hydrogen storage: enhancing kinetics and eliminating ammonia, *J. Am. Chem. Soc.* 132(2010) 1490-1491.

[54] S. F. Li, Y. H Guo, W. W. Sun, D. L. Sun, and X. B. Yu, Platinum nanoparticle functionalized CNTs as nanoscaffolds and catalysts to enhance the dehydrogenation of ammonia-borane, *J. Phys. Chem. C* 114(2010)21885-21890.

[55] Li Li *et al.* Lithium-catalyzed dehydrogenation of ammonia borane within mesoporous carbon framework for chemical hydrogen storage, *Adv. Funct. Mater.*

19(2009)265-271.

[56] Gadipelli Srinivas, Jamie Ford, Wei Zhou, Taner Yildirim, Zn-MOF assisted dehydrogenation of ammonia borane: enhanced kinetics and clean hydrogen generation, *International Journal of Hydrogen Energy* 37(2012)3633-3638.

[57] Jiapeng Zhang, Jiang Li, Lijing Yang, Ran Li, Fengming Zhang, Hua Dong, Efficient hydrogen production from ammonia borane hydrolysis catalyzed by TiO₂-supported RuCo catalysts, *International Journal of Hydrogen Energy*, 46(2021)3964-3973

[58] Yating He , Yumei Peng , Yi Wang *, Yan Long, Guangyin Fan, Air-engaged fabrication of nitrogen-doped carbon skeleton as an excellent platform for ultrafine well-dispersed RuNi alloy nanoparticles toward efficient hydrolysis of ammonia borane, *Fuel* 297 (2021) 120750(1-11).

[59] Martin E. Bluhm, Mark G. Bradley, Robert Butterick, Upal Kusari, and Larry G. Sneddon, Amineborane-based chemical hydrogen storage: enhanced ammonia borane dehydrogenation in ionic liquid, *J. Am. Chem. Soc.* 128(2006)7748-7749.

[60] Daniel W. Himmelberger, Chang Won Yoon, Martin E. Bluhm, Patrick J. Carroll, and Larry G. Sneddon, Base-promoted ammonia borane hydrogen-release, *J. Am. Chem. Soc.* 131(2009)14101-14110.

[61] Yanping Huang *et al.* Experimental verification of the high pressure crystal structures in NH₃BH₃, *J. Chem. Phys.* 140(2014)244507(1-9).

[62] Zaixing Yang, Yan Wang, Jing Liang and Jun Chen, Hydrogen releasing of lithium amidoborane-LiNH₂BH₃, *Materials Transactions*, 52(2011)651-653.

[63] Charles W. Hamilton, R. Tom Baker, Anne Staubitz and Ian Manners, BCN compounds for chemical hydrogen storage, *Chem. Soc. Rev.* 38(2009) 279-293).

[64] Serdar Akbayrak and Saim Özkar, Ruthenium(0) nanoparticles supported on Mmltiwalled carbon nanotube as highly active catalyst for hydrogen generation from ammonia–borane, *ACS Appl. Mater. Interfaces* 4(2012)6302–6310.

[65] Jun-Min Yan, Xin-Bo Zhang, Song Han, Hiroshi Shioyama, and Qiang Xu, Iron-nanoparticle-catalyzed hydrolytic dehydrogenation of ammonia borane for chemical hydrogen storage, *Angew. Chem. Int. Ed.* 47(2008)2287 –2289.

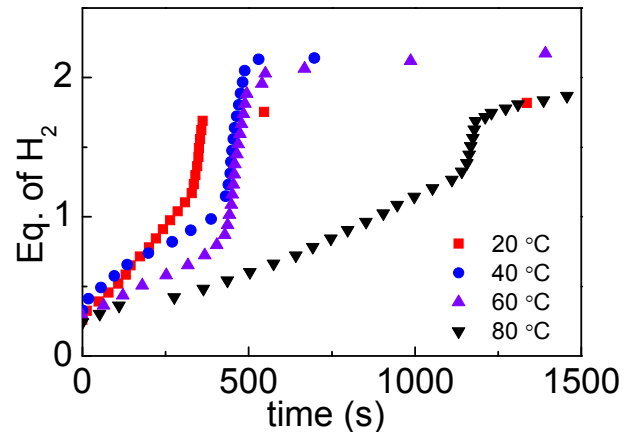


Figure 1: The time dependence of released equivalents of hydrogen (abbreviated to “Eq. of H₂”) from ammonia borane, which is induced by electrical breakdown at different temperatures: i) the red squares 20 °C, ii) the blue circles 40 °C, iii) the purple triangles 60 °C, iv) the black reverse triangles 80 °C.

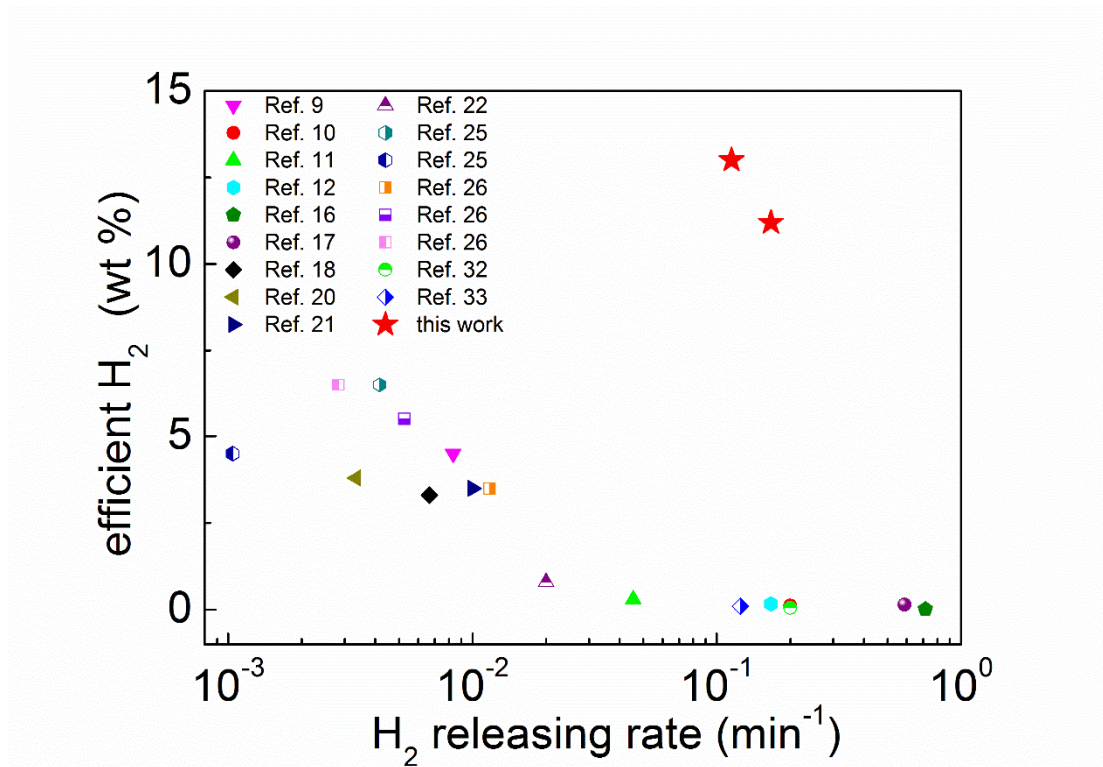


Figure 2: The hydrogen releasing rate (min⁻¹) versus the efficient hydrogen storage weight percentage (wt %) reported in the previous work [9-12, 16-18, 20-22, 25, 26, 32, 33] and this work.

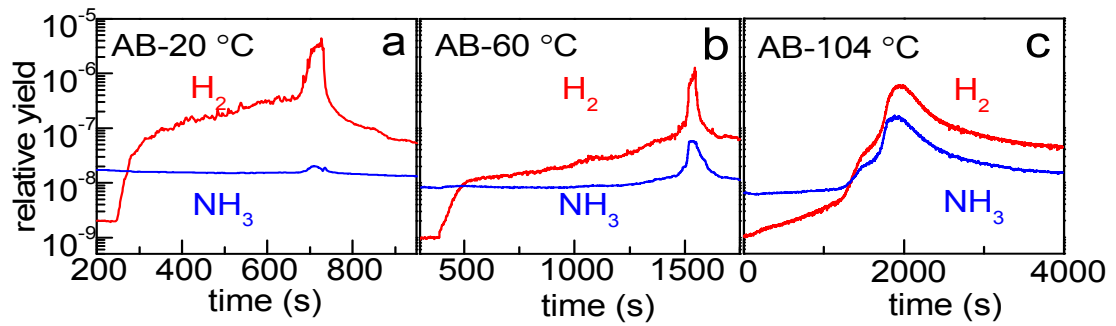


Figure 3: Mass Spectroscopy: Time dependence of the relative yield of the released gases from ammonia borane at temperatures; (a) 20 °C under electrical breakdown; (b) 60 °C under electrical breakdown; (c) thermolysis at 104 °C. The red lines give the time dependence of hydrogen $m/e=2$ releasing process and the blue lines give the time dependence of ammonia $m/e=17$ releasing process, respectively.

Supplementary Information

Shock Initiation of Explosives through Shock Wave-Induced Electrical Breakdown

Yuanjie Huang^{1,2}, Zhiqiang Chen^{2*}

¹ *Chinese Academy of Engineering Physics, Mianyang 621900, China*

² *Center for High Pressure Science and Technology*

Advanced Research, Shanghai 201203, China

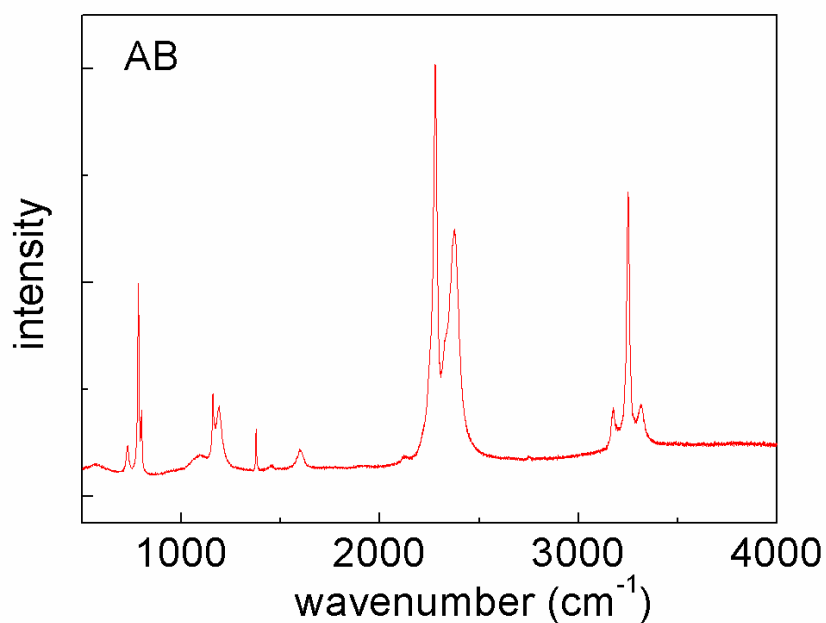


Figure S1. The Raman spectrum of pristine ammonia borane at room temperature.

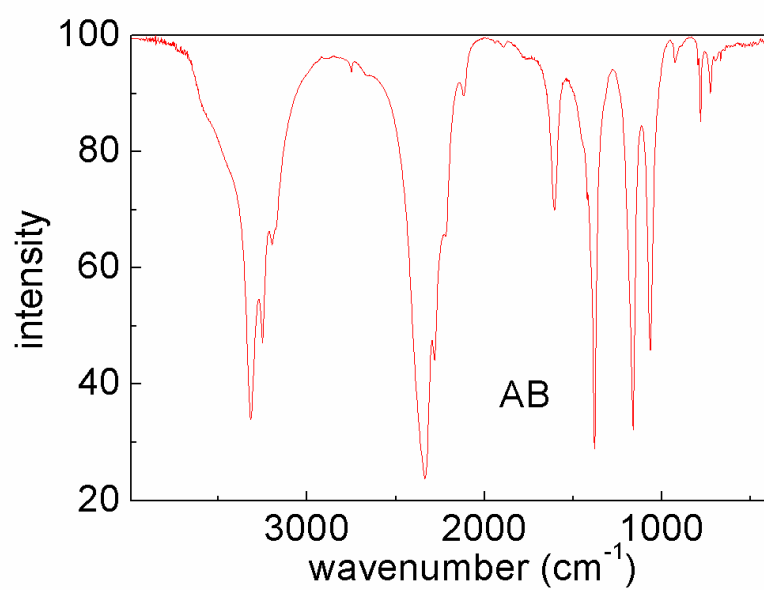


Figure S2. Fourier Transform infrared spectroscopy (FTIR) of pristine ammonia borane at room temperature.

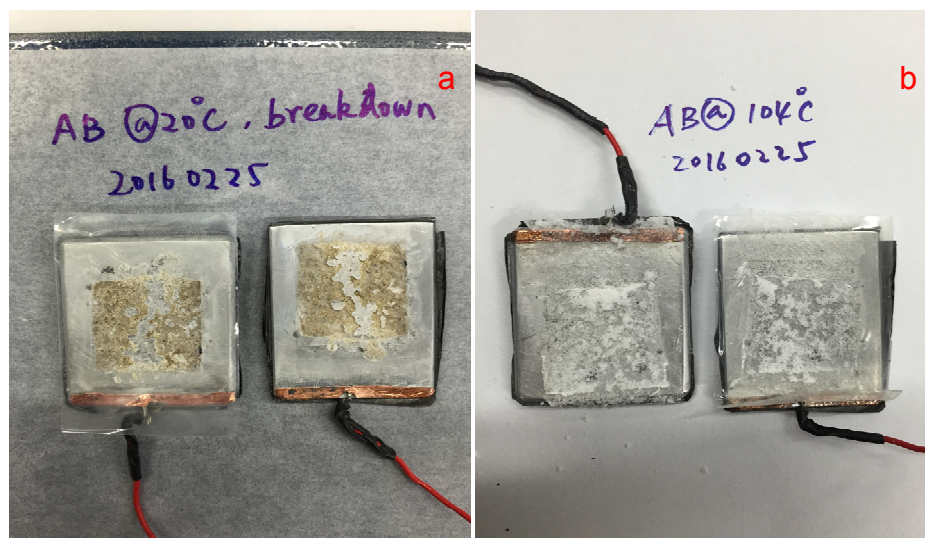


Figure S3. The images of recovered products of NH_3BH_3 under the electrical breakdown and thermal decomposition: (a) electrical breakdown at 20 °C; (b) thermal decomposition at 104 °C.

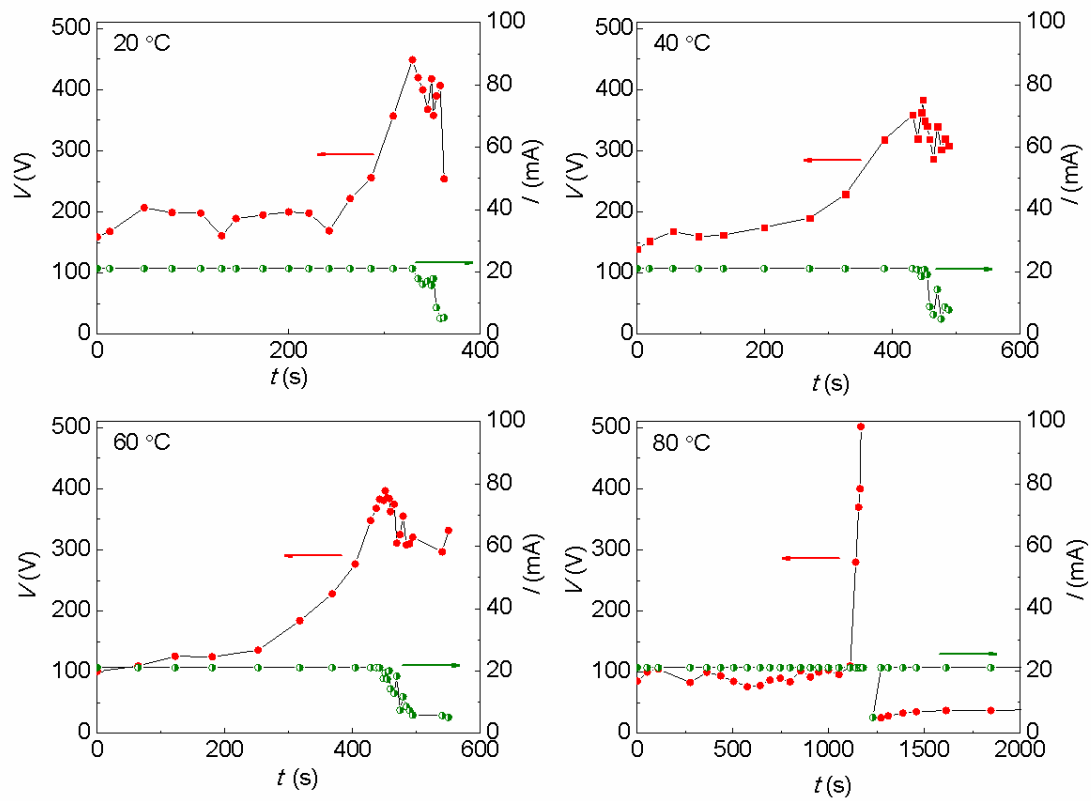


Figure S4. Time dependence of electric breakdown voltage and the current at different temperatures 20 °C, 40 °C, 60 °C and 80 °C. The red circles denote the voltages and the half-green circles denote the currents.